UCRL-51975

MEDIUM PROPERTIES AND TOTAL ENERGY COUPLING IN UNDERGROUND EXPLOSIONS

Stephan R. Kurtz

December 15, 1975

Prepared for U.S. Energy Research & Development Administration under contract No. W-7405-Eng-48

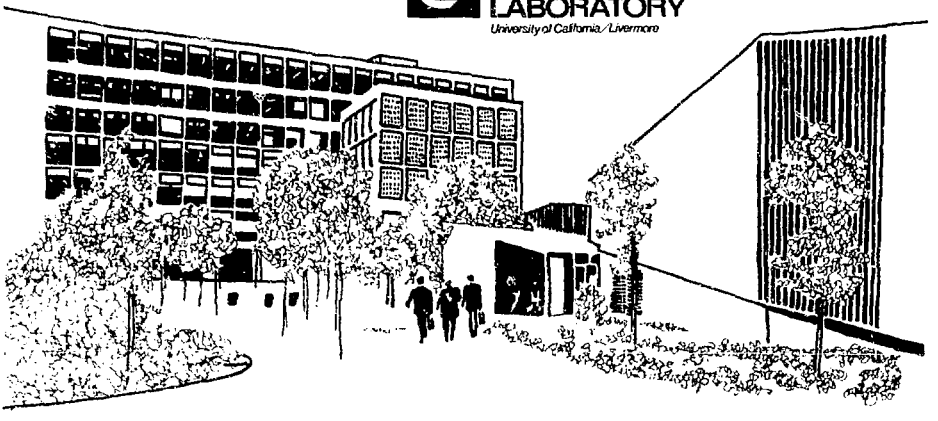

Printed in the United States of America
Available from
National Technical Information Service
U.S. Department of Commerce
5285 Port Royal Road
Springfield, Virginia 22151
Price: Printed Copy $___*; Microfiche $2.25

*Pages	NTIS Selling Price
1-50	$4.00
51-150	$5.45
151-325	$7.60
326-500	$10.60
501-1000	$13.60

Distribution Category
UC-35

LAWRENCE LIVERMORE LABORATORY
University of California / Livermore, California / 94550

UCRL-51975

MEDIUM PROPERTIES AND TOTAL ENERGY COUPLING IN UNDERGROUND EXPLOSIONS

Stephan R. Kurtz

MS. Date: December 15, 1975

Contents

MEDIUM PROPERTIES AND TOTAL ENERGY COUPLING IN UNDERGROUND EXPLOSIONS

Abstract

A phenomenological model is presented that allows the direct calculation of the effects of variations in medium properties on the total energy coupling between the medium and an underground explosion. The model presented is based upon the assumption that the shock wave generated in the medium can be described as a spherical blast wave at early times. The total energy coupled to the medium is then simply the sum of the kinetic and internal energies of this blast wave. Results obtained by use of this model indicate that the energy coupling is more strongly affected by the medium's porosity than by its water content. These results agree well with those obtained by summing the energy deposited by the blast wave as a function of range.

Introduction

Knowledge of how much energy is coupled into the surrounding medium by an underground explosion can be of importance in such areas as the containment of underground nuclear explosions, seismic evasion analysis, prediction of chemical processes in the rock surrounding the explosion, seismic surveys, and various energy programs such as in situ coal gasification. This makes it important to determine how medium properties such as porosity and water content influence this energy coupling.

Energy coupling between a tamped explosion and the surrounding medium can be separated into two phases. First, there is the prompt coupling of energy associated with the formation of a shock wave in the medium. The second phase is associated with the coupling of energy from the shock wave to the medium as the wave travels outward depositing energy into the medium by doing PdV work on the rock, successively vaporizing, melting, and displacing the medium.

The first phase of energy coupling takes place in a very short time interval (a few tens to hundreds of

microseconds) with the second phase lasting about a thousand times as long. The high temperatures and pressures resulting from the sudden energy release of an underground explosion initiate a shock wave in the medium surrounding the explosion chamber. One-dimensional source calculations indicate that this shock wave approaches a spherical blast wave type configuration when the radius of the shock front is approximately twice the initial radius of the explosion chamber.

We will consider the first phase of energy coupling to be complete when a spherical blast wave can be used to describe the ground shock. It is the energy associated with this blast wave that is available for deposition in the medium during the second phase of energy coupling. This energy is not, of course, 100% of the explosion's total energy. Much energy was expended simply in the blast wave's formation. Also, a large fraction of the explosion's energy is contained in the low density, high temperature cavity behind the blast wave.

Previous work has focussed primarily on the second phase of energy coupling. In particular, this prior work has addressed the effects of medium properties on the propagation and attenuation of a given initial shock wave.[1,2] Some attention has also been paid to the influence of medium properties on the energy deposition to the medium by the shock wave as a function of range.[3,4] However, none of this previous work directly addresses the question of how much of the explosive energy was coupled to the shock wave (blast wave) initially and what effects the medium properties have upon this coupling. Some experimental work[5,6] is presently being carried out in this area, but as yet no definitive results have been reported. Although the energy deposition to the medium during phase two of coupling is of the ultimate importance after all is said and done, it remains true that only the energy that is available in the blast wave initially can be deposited. It therefore seems fitting to pay some attention to the influence of medium properties on the energy available in the ground shock (blast wave) at the end of the first phase of energy coupling.

In this paper we present a model that allows us to calculate directly the effects upon the prompt coupling of energy to the ground shock of variations in medium properties. This model is phenomenological in nature and is based upon the assumption that the explosion-induced shock wave can be described as a blast wave at early times. The energy coupled is then simply the sum of the kinetic and internal energies of this blast wave. Results obtained by use of this model

indicate that the energy coupled into the blast wave is affected more strongly by porosity than by water content.

Model Definition

In a simple blast wave model, we assume that essentially all of the mass of the surrounding medium that has been swept out by the blast wave is contained in a thin layer of thickness Δr immediately behind the leading surface of the shock front. That is, the outgoing shock wave can be characterized as a thin shell of highly compressed material propagating out from the explosion point with shock velocity V_s (see Fig. 1). The total energy associated with the blast wave is then simply the sum of the kinetic and internal energies of the material making up the blast wave shell. That is:

$$E = \frac{1}{2} MU^2 + MI \qquad (1)$$

where M is the mass swept out by the diverging shock wave, U is the peak particle velocity of the material immediately behind the shock front, and I is the specific internal energy of the material behind the shock front.

Because of the very high pressures being considered, the equation of

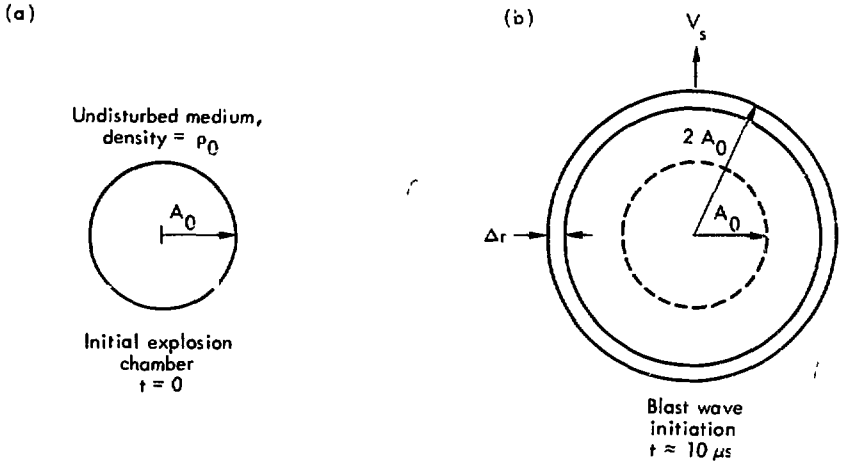

Fig. 1 Schematic representation of blast wave function.

state of the surrounding medium can be expressed in the following form[7,8]:

$$P_s = (\gamma-1)\rho\, I \qquad (2)$$

where P_s is pressure, ρ is density, I is again the specific internal energy, and γ is a dimensionless parameter. (Equation (2) is similar to the Mie-Gruneisen equation of state for solids if the Gruneisen coefficient Γ is set equal to $(\gamma-1)$.) Strong shock relationships then allow us to express U and I in terms of the shock velocity V_s and shock pressure P_s as follows:

$$U = \frac{2}{\gamma+1} V_s \,, \qquad (3)$$

$$I = \frac{P_s}{(\gamma-1)\rho} = \frac{P_s}{(\gamma-1)\rho_0\left(\frac{\gamma+1}{\gamma-1}\right)} = \frac{P_s}{\rho_0(\gamma+1)} \,, \qquad (4)$$

where ρ_0 is the initial *in situ* density of the surrounding medium.

If we now express M by:

$$M = \frac{4}{3}\pi R_s^3 \rho_0 \qquad (5)$$

where R_s is the range of the shock front from the explosion point, then substituting Eqs. (3), (4), and (5) into Eq. (1) results in:

$$E = \frac{1}{2}\left(\frac{4}{3}\pi R_s^3 \rho_0\right)\left(\frac{2}{\gamma+1} V_s\right)^2 + \left(\frac{4}{3}\pi R_s^3 \rho_0\right)\left(\frac{P_s}{\rho_0(\gamma+1)}\right)$$

$$= \frac{8}{3}\pi R_s^3 \rho_0 \left(\frac{1}{\gamma+1}\right)^2 V_s^2 + \frac{4}{3}\pi R_s^3 \left(\frac{1}{\gamma+1}\right) P_s \,. \qquad (6)$$

Previous work[9,10] on the development of the BOTE ground motion model presents the following expressions for the position R_s, velocity V_s, and pressure P_s of a spherical blast wave as functions of both range and time:

$$R_s = R_{s0}\left(\frac{\gamma}{\rho_0}\right)^{1/5} t^{2/5} \qquad (7)$$

$$V_s = \begin{cases} V_{s1}\left(\frac{\gamma}{\rho_0}\right)^{1/2} R_s^{-3/2} \\ V_{s2}\left(\frac{\gamma}{\rho_0}\right)^{1/5} t^{-3/5} \end{cases} \qquad (8)$$

$$P_s = \begin{cases} P_{s1}(\gamma) R_s^{-3} \\ P_{s2}(\rho_0)^{3/5}(\gamma)^{2/5} t^{-6/5} \end{cases} \qquad (9)$$

where Y is the explosive yield and

$$R_{s0} \equiv \left(\frac{5}{2}\right)^{2/5} \Psi^{2/5} \qquad (10)$$

$$V_{s1} \equiv \Psi \qquad (11)$$

$$V_{s2} = \left(\frac{5}{2}\right)^{-3/5} \psi^{2/5} \qquad (12)$$

$$P_{s1} = \left(\frac{2}{\gamma+1}\right) \psi^2 \qquad (13)$$

$$P_{s2} = \left(\frac{2}{\gamma+1}\right)\left(\frac{5}{2}\right)^{-6/5} \psi^{4/5} \qquad (14)$$

with ψ being defined by

$$\psi = \left[\frac{3}{4\pi} \frac{(\gamma-1)(\gamma+1)^2}{(3\gamma-1)}\right]^{1/2} . \qquad (15)$$

Noting that $V_s(t)$ can be also expressed as

$$V_s(t) = \frac{2}{5} \frac{R_s(t)}{t} \qquad (16)$$

and then substituting $R_s(t)$ and $P_s(t)$ from Eqs. (7) and (9) back into Eq. (6), we find after simplification that the total energy E in the blast wave can be expressed as

$$E = 4 \left[\frac{\gamma-1}{3\gamma-1}\right] Y \quad . \qquad (17)$$

Dividing both sides of Eq. (17) by Y gives the following expression for the fraction of explosive yield coupled to the ground shock

$$\frac{E}{Y} = 4 \left[\frac{\gamma-1}{3\gamma-1}\right] \quad . \qquad (18)$$

Equation (18) relates the explosive yield Y to the energy coupled to the blast wave in terms of the dimensionless parameter γ. Previous work[11,12] has shown that γ can be expressed in terms of the total porosity ϕ (expressed as a volume fraction) of the medium and the weight fraction of water W present in the medium by:

Table 1 The substitutions necessary to obtain expressions γ in terms of various pairs of variables describing the medium. In all cases, begin with the expression for $\gamma(W,\phi)$ shown in Eq. (19).

To get	Replace ϕ by	Replace W by
$\gamma(W,\phi)$	ϕ	W
$\gamma(W,\phi_g)$	$\left[\frac{\phi_g - W\phi_g + \rho_g W}{1 - W\rho_g - W}\right]^*$	W
$\gamma(K,\phi)$	ϕ	$\left[\frac{K\phi}{K\phi + \rho_g (1-\phi)}\right]^*$
$\gamma(K,\phi_g)$	$\left[\frac{\phi_g}{1 - K}\right]$	$\left[\frac{K\phi_g}{K\phi_g + \rho_g (1-K-\phi_g)}\right]^*$

*$\rho_g \equiv$ grain density of the material.

$$\gamma = (0.4)\ W + (1-W)\left[\frac{2\ S}{1-\phi} - 1\right][1-\phi]^5 + 1 \qquad (19)$$

where S is the slope of a linear fit to the shock velocity, particle velocity Hugoniot for the dry, nonporous matrix material in the medium (i.e., $V_s = SU + C$). The combination of Eq. (18) and (19) now allows us to determine the influence of variations in total porosity and water content on the amount of energy initially coupled to the ground shock by an underground explosion. In order to determine the effects of variations in other medium properties such as saturation K (= $\phi_0 W/\phi$) or gas fill porosity ϕ_g (= $\phi - \phi_0 W$),* we need only to rewrite γ in terms of whichever pair of variables we are interested in. Table 1 indicates the substitutions required to do this.

*The expression $\phi_g = \phi - \phi_0 W$ assumes that the density of water = 1.

Results

In this section we wish to demonstrate how the model just described can be used to determine the influence of variations in medium properties on the initial energy coupled to the ground shock (and so available for ultimate deposition in the medium). As input we will use the data shown in Table 2 which represents average explosion point medium properties for underground nuclear tests executed in Yucca Flat at the Nevada Test Site.[13] Figures 2-9 show how the energy in the ground shock, expressed as a fraction of the explosive yield (i.e., E/Y), varies as the medium properties are varied. Figures 2 and 3 show the influence of the variations in water content and total porosity. Figures 6 and 7 show the effects of variations in water content and gas fill porosity. Figures 8 and 9 show the effect of variations in saturation and gas fill porosity.

From Figs. 2-9, we see that the fraction of explosive energy coupled into the ground shock varies between 0.35 and 0.55 (35-55%) depending upon the set of medium properties assumed. This result is in good agreement with that obtained by simply adding together the energies required to vaporize, melt, and displace the medium. (See Appendix A for details.) More importantly, Figs. 2-9 demonstrate the effect of holding one medium property (e.g. total porosity) constant while varying another property (e.g. saturation).

In particular, Figs. 2-5 show that increasing total porosity while holding water content or saturation fixed

results in less energy being coupled. Conversely, increasing water content or saturation while holding total porosity fixed results in increased

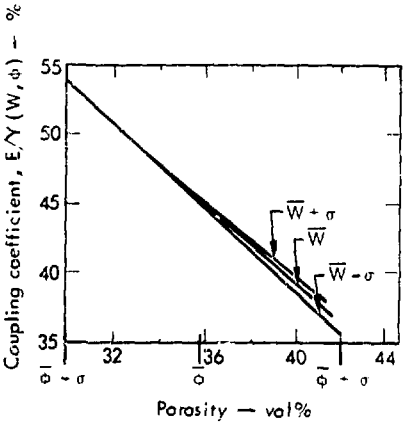

Fig. 2 Variation of the coupling coefficient, E/Y (the ratio of the energy coupled into the shock wave to the total explosive yield) plotted for fixed values of water content, W, and varying porosity, ϕ. Each of the parameters has a range of ± one standard deviation, σ, from its mean value listed in Table 2.

Table 2 Average explosion point medium properties for underground nuclear tests executed in Yucca Flat at the Nevada Test Site.[13] Note that the values of ϕ, ϕg, W, and K are listed below as percentages. These values must be converted to decimal fractions (i.e., divide by 100) when they are used in Eq. (19) or any of the expressions listed in Table 1.

Property	Mean value	Standard deviation
Total porosity (ϕ) (vol %)	35.9	±6.2
Water content (W) (wt %)	12.3	±4.0
Saturation (K) (vol %)	64.5	±18.1
Gas-fill porosity (ϕ_g) (vol %)	12.75[a]	
In situ density (ρ_0) (Mg/m^3)	1.79	±0.19
Grain density (ρ_g) (Mg/m^3)	2.45[b]	

[a] Calculated using $\bar{\phi}_g = \bar{\phi}\left(1 - \frac{\bar{K}}{100}\right)$

[b] Calculated using $\bar{\rho}_g = \bar{\rho}_0 \left(\frac{1 - \bar{W}/100}{1 - \bar{\phi}/100}\right)$.

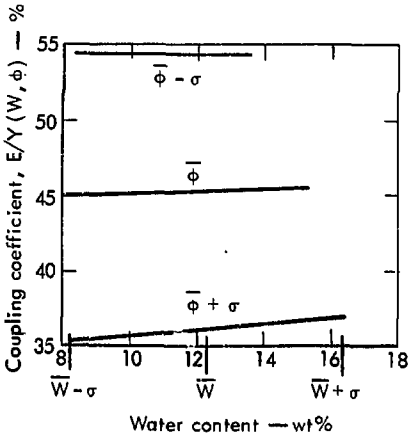

Fig. 3 Variation of the coupling coefficient, E/Y, for fixed values of porosity and varying water content. Each parameter ranges one standard deviation, ±σ, from its mean value listed in Table 2.

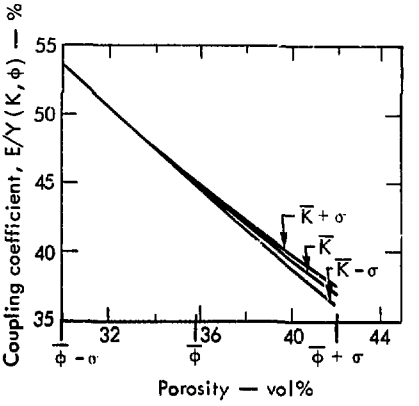

Fig. 4 Variation of the coupling coefficient, E/Y, for fixed values of saturation, K, and varying porosity. Each parameter ranges one standard deviation from its mean value listed in Table 2.

coupling. That is what would intuitively be expected. Figs. 6-9 show that increasing gas fill porosity while holding saturation or water content fixed also results in decreased coupling. Again this is as expected. More interesting is the result that increasing saturation or water content while holding gas fill porosity fixed also results in decreased coupling. This seems to be just the opposite of what one would expect. However, this effect is easily explained by noting that in order to increase the water

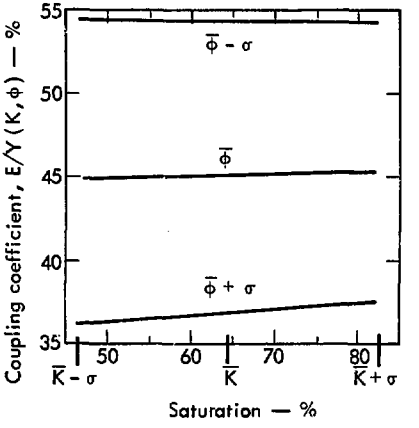

Fig. 5 Variation of the coupling coefficient, E/Y, for fixed values of porosity and varying saturation. Each parameter ranges one standard deviation from its value listed in Table 2.

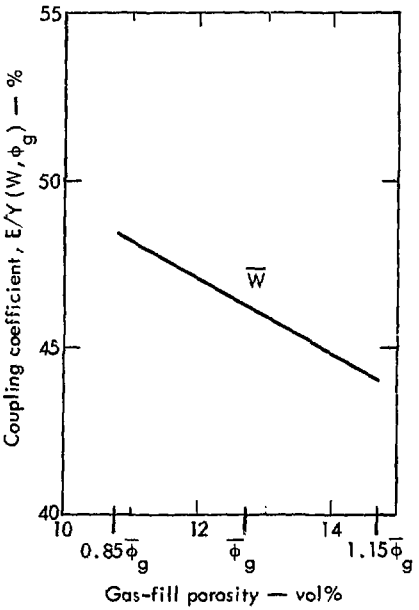

Fig. 6 Variation of the coupling coefficient, E/Y, for varying gas-fill porosity, ϕ_g, and constant water content. The gas-fill porosity varies ±15% from its mean value listed in Table 2.

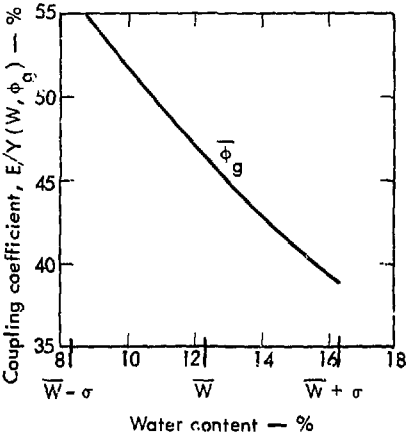

Fig. 7 Variation of the coupling coefficient, E/Y, for fixed gas-filled porosity and variable water content. The range of variation is one standard deviation from the mean value listed in Table 2.

content or saturation of the medium while holding the gas filled porosity fixed, one must increase the total porosity of the medium also. And, as seen in Figs. 2-5, increasing total porosity decreases the coupling much faster than increasing the water content or saturation increases it.

Further examples of the influence of variations in medium properties on the energy coupled to the ground shock are shown in Appendix B.

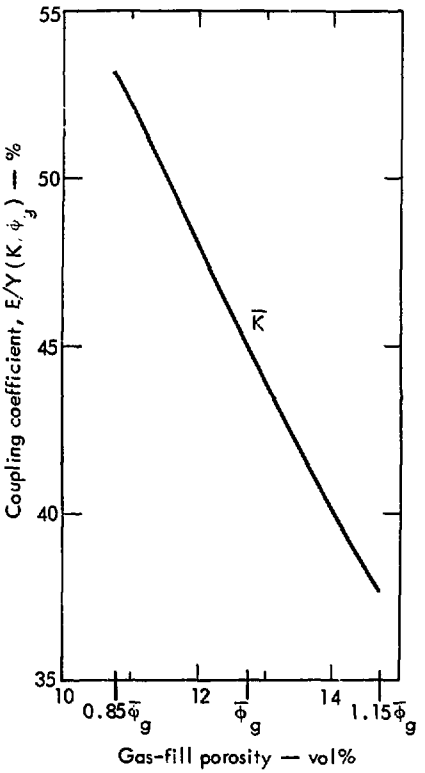

Fig. 8 Variation of the coupling coefficient, E/Y, for fixed saturation and varying gas-filled porosity. The variation in ϕ_g is ±15% from the mean value listed in Table 2.

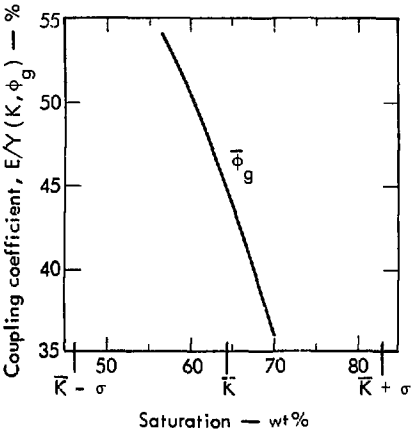

Fig. 9 Variation of the coupling coefficient, E/Y, for fixed gas-filled porosity and varying saturation. The range of variation is one standard deviation from the mean value listed in Table 2.

Discussion

Energy coupled to the medium is of importance in a number of different areas: containment of underground nuclear explosions; seismic evasion analysis; prediction of chemical processes in the rock surrounding the explosion; seismic surveys; and various energy programs such as in situ coal

gasification. The shock wave that emanates from the explosion point represents the primary means by which an underground explosion couples energy to the surrounding medium as it deposits its energy by doing PdV work on the rock. Previous work[1-4] has addressed the question of how medium properties such as porosity and water content influence the coupling between the shock wave and the medium. In this paper, we have addressed a question that we feel to be of equal importance, i.e. what influence do these medium properties have upon the energy coupled from the explosion to the shock wave initially.

This paper presents a phenomenological model, rather than one based on any first-principles arguments. However, this rather simple model provides good agreement with those results that can be extracted from previous work. Our model has the advantage of requiring neither extensive knowledge of the medium's equation of state nor large amounts of computer time in order to evaluate the effects of variations in medium properties or to look at the effects of explosions in different media.

It should be emphasized, however, that this model ignores the questions of how medium properties affect the coupling between the medium and the shock wave, or how the energy ultimately coupled to the medium is split between kinetic and internal energies. Therefore it cannot replace computer studies for a detailed analysis of the coupling between an explosion and the surrounding medium. It can, however, provide a quick and easy means of evaluating the gross effects of medium properties on initial energy coupling.

References

1. B. K. Crowley, Int. J. Rock Mech. Mining Sci. 10 (5), 437 (1973).
2. T. R. Butkovich, Effects of Water Saturation on Underground Nuclear Detonations, Lawrence Livermore Laboratory, Rept. UCRL-51110 (1970).
3. T. R. Butkovich, The Gas Equation of State for Natural Materials, Lawrence Livermore Laboratory, Rept. UCRL-14729 (1967).
4. T. R. Butkovich, Rock Melt from an Underground Nuclear Explosion, Lawrence Livermore Laboratory, Rept. UCRL-51554 (1974).
5. D. B. Larson and H. C. Rodean, The Relationship of Material Properties to Seismic Coupling Part 1: Shock Wave Studies of Rock and Rock-Like Materials, Lawrence Livermore Laboratory, Rept. UCRL-51769 (1975).
6. D. B. Larson, "Rock Mechanics: A Review of Current Research," in Lawrence Livermore Laboratory Energy and Technology Review July 1975, R. B. Carr, Ed., Lawrence Livermore Laboratory, Rept. UCRL-52000-75-7 (1975).
7. J. P. Mutachlecner and B. R. Saunders, Hydrodynamic Measurements of Yields of Underground Tests During Niblick, Whetstone, and Flintlock, Los Alamos Scientific Laboratory, Los Alamos, New Mexico, Rept. LA-3971 (1968)(title U, report SRD).
8. W. J. Rae, "Impact-Generated Shock Propagation," in High Velocity Impact Phenomena, R. Kinslow, Ed. (Academic Press, New York, 1970) pp. 215-291.
9. S. R. Kurtz, The BOTE Model: An Analytic Approach to Predicting Ground Motion Phenomena Resulting from Underground Nuclear Explosion, Lawrence Livermore Laboratory, Rept. UCRL-51471 (1973).
10. S. R. Kurtz, J. Geophys. Res. 80 (32), 4449 (1975).
11. S. R. Kurtz, An Approximate Method for Determining the Influence of Water and Porosity on the Gruneisen Gamma, Lawrence Livermore Laboratory, Rept. UCRL-76010 (1975).
12. S. R. Kurtz, The Zero-Pressure Gruneisen Coefficient for Wet, Porous Media, Lawrence Livermore Laboratory, Rept. UCRL-51896 (1975).
13. N. Howard, Lawrence Livermore Laboratory, Internal Documents UOPKB 75-110 (1974) and UOPKB 74-102 (1974). Readers outside the Laboratory who desire further information on LLL internal documents should address their inquiries to the Technical Information Department, Lawrence Livermore Laboratory, Livermore, California 94550.

APPENDIX A: AN ALTERNATE APPROACH TO DETERMINING TOTAL ENERGY COUPLING

The shock wave that emanates from the explosion point deposits its energy into the medium by successively vaporizing, melting, and displacing the rock. This implies that the total energy E initially contained in the shock wave can be expressed as:

$$E = \varepsilon_V + \varepsilon_M + \varepsilon_C + \varepsilon_E \tag{A1}$$

where ε_V is the energy deposited due to vaporization of the medium, ε_M is the energy deposited due to melting, ε_C is the energy deposited while the stress wave is crushing and cracking the medium, and ε_E is the energy deposited during the elastic phase of the stress wave's lifetime.

The vaporization energy, ε_V, can be determined from the work of Butkovich[3] on the influence of medium properties on the amount of material vaporized. Butkovich found that the radius R_V of the sphere of material that would be dynamically shock vaporized by an underground explosion could be expressed as:

$$R_V = 1.524\ e_V^{-0.256}\ (Y)^{1/3} \tag{A2}$$

where R_V is expressed in meters, Y is the explosive yield in kilotons, and e_V is the energy of vaporization in units of 10^{12} erg/cm^3. Solving Eq. (A2) for e_V and multiplying by the volume of the vaporized sphere results in:

$$\varepsilon_V = e_V\ V_V = \left[\frac{(Y)^{1/3}\ 1.524}{R_V}\right]^{1/0.256} \frac{4}{3}\pi(R_V)^3 \tag{A3}$$

where V_V must be expressed in terms of cubic centimeters in order to balance the equation. Noting that R_V may also be expressed as:

$$R_V = R_V^{1kt}\ (Y)^{1/3}\ , \tag{A4}$$

where R_V^{1kt} is the radius of vaporization due to an explosive yield of one kiloton of energy (see Table A1 for values for R_V^{1kt}), we find upon substituting Eq. (A4) into Eq. (A3) that

$$\varepsilon_V = \left[\frac{1.524}{R_V^{1kt}}\right]^{1/0.256} \frac{4}{3}\pi\left(R_V^{1kt}\right)^3\ Y\ . \tag{A5}$$

Hence the energy deposited in the medium while the shock wave is vaporizing the rock varies linearly with the explosive yield. Table A2 lists e_V, ε_V, and ε_V/Y for various explosion point media.

The amount of explosive yield deposited in the rock melted by an underground explosion has been studied by Butkovich[4] for explosion point media of different assumed *in situ* densities and melt temperature. Butkovich's results are shown in Fig. A1 and Table A3. It should be noted that Butkovich was interested in determining the total amount of rock melted by an underground explosion, not just that which is dynamically shock melted. So, in addition to shock melting, Butkovich attempted to include the effects of other heat transfer mechanisms that could melt more rock: e.g., blow-off of the cavity wall during the later part of cavity expansion and mixing with the high temperature cavity contents; the heat transfer to the already warm wall by means of radiation and convection, raising the temperature to the melting point, with the

Table A1 Values R_V^{1kt} for various explosion point media.[3]

Media	*In situ* density (Mg/m^3)	R_V^{1kt} (m)
Granite	2.66	1.83
Saturated tuff	1.97	2.06
Dry tuff	1.76	2.15
Alluvium	1.60	2.20

Table A2 Values of e_V, ε_V, and ε_V/Y for various explosion point media. An explosive yield of 1kt (4.186×10^{19} erg) was assumed in all cases.

Media	e_V (10^{12} erg/cm^3)	ε_V (10^{19} erg)	ε_V/Y
Granite	0.489	1.256	0.30
Saturated tuff	0.308	1.128	0.269
Dry tuff	0.261	1.085	0.259
Alluvium	0.238	1.063	0.254

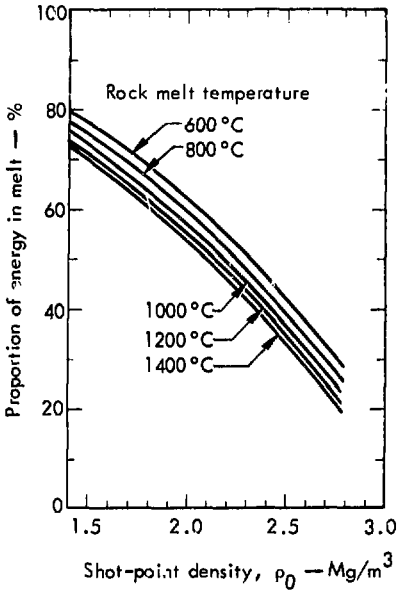

Fig. A1 Total fraction of explosive yield taken up in rock melt vs shot-point density, assuming different melting temperatures. (Taken from Ref. 4.)

Table A3 Total percentage of explosive energy in rock melt for rocks of different explosion-point densities and assuming different melt temperatures.

ρ_0(Mg/m^3)	1400°C	1200°C	1000°C	800°C	600°C
1.4	73.03	74.45	76.03	77.84	79.97
1.6	66.85	68.39	70.13	72.13	74.57
1.8	60.31	61.94	63.79	65.94	68.52
2.0	53.74	55.41	57.37	59.54	62.25
2.2	45.86	47.57	49.53	51.83	54.65
2.4	37.71	39.43	41.39	43.71	46.59
2.6	28.75	30.44	32.39	34.71	37.60
2.8	18.79	20.44	22.35	24.64	27.52

Table A4 Total mass of rock melted for rocks of different densities (ρ_0) and different assumed melt temperatures and enthalpies (ΔH_{melt}). Taken from Ref. 4.

	Mass (metric tons/kt) at temperature and enthalpy (cal/g)				
ρ_0(Mg/m^3)	1400°C 449	1200°C 393	1000°C 336	800°C 280	600°C 224
1.4	1656	1894	2263	2780	3570
1.6	1489	1770	2087	2576	3327
1.8	1343	1576	1899	2355	3058
2.0	1197	1410	1706	2126	2779
2.2	1021	1210	1474	1851	2440
2.4	840	1003	1282	1561	2080
2.6	640	775	964	1280	1679
2.8	418	520	665	880	1229

melt running or raining down under the influence of gravity, exposing more material to the hot cavity environment. These other mechanisms result in significantly more rock being melted than that due solely to shock melting. In particular, Butkovich states that while the rock dynamically shock melted per kiloton of explosive yield is approximately 350 metric tons, the total melt appears to range from about 1300 metric ton/kt to two to three times this amount. Table A4 lists Butkovich's results for total mass melted.

The amount of energy ϵ_M associated with the dynamic shock melting of medium can be determined by finding what fraction of the total melt 350 metric tons/kt represents and then multiplying the total energy in the melt (see Table A3) by this fraction. The results of this operation are shown in Table A5 and indicate that ϵ_M is independent of initial material density and is only affected by the assumed material melt temperature.

Table A5 Percentage of explosive energy associated with the dynamic shock melting of rocks of different explosion point densities and assuming different melt temperatures.

ρ_0(Mg/m^3)	1400°C	1200°C	1000°C	800°C	600°C
1.4-2.8	15.72	13.76	11.76	9.80	7.84

After the stress wave has decayed to a point where it can no longer deposit enough energy to the medium to melt the rock, it continues to lose energy to the medium by crushing and cracking the rock. This energy ε_C is rather difficult to quantify, but private communication with J. M. Thomsen indicates that ε_C is on the order of 5-10% of the explosive yield for tuff and alluvium.

The energy ε_E remaining in the stress wave after it has gone elastic has been determined to be on the order of 1% of the explosive yield.[A1-3] In particular, Perrett[A1] has shown that for explosions in alluvium only about 0.04% of the explosive yield is contained in the elastic phase of the stress wave. Equivalent values for other media are 0.06% for explosions in dry tuff, 2% for explosions in dolomite and alternating shale/sandstone layer, and about 3% for explosions in salt.

As an indication of how much energy is represented by the sum of ε_V, ε_M, ε_C, and ε_E we will assume a tuff or alluvium-type medium and that ε_V/Y ranges from 0.254 to 0.269 (see Table A2), ε_M/Y ranges from 0.078 to 0.157 (see Table A5), ε_C/Y ranges from 0.05 to 0.10, and ε_E/Y ranges from 0.0004 to 0.0006. The result of using the above values in Eq. A1 is that E/Y is seen to range between 0.38 to 0.53. This range of values for E/Y is in good agreement with that displayed in Figs. 2-9.

REFERENCES

A1. W. R. Perrett, Free-Field and Surface Motion from a Nuclear Explosion in Alluvium: MERLIN Event, Sandia Laboratories, Albuquerque, New Mexico, Rept. WT-1529 (1961).

A2. V. N. Radionov, V. V. Aduckkin, V. N. Kostyuckenko, V. N. Nikolaevskii, A. N. Ramashov, and V. M. Tsvetkov, Mechanical Effect of an Underground Explosion, M. A. Sadovskii, Ed., available as Lawrence Livermore Laboratory Rept. UCRL-Trans-10676 (1972).

A3. V. P. Korgavov, Engl. ed. Izvestia, Acad. Sci., USSR, Physics of the Solid Earth, 10, 653 (1974).

APPENDIX B ENERGY COUPLED TO THE GROUND SHOCK BY AN EXPLOSION IN SILICATE ROCK

In this section, we will look in particular at the energy coupled into the ground shock by an underground explosion taking place in a medium composed of silicate type rock. Expressing the coupled energy as a fraction of the explosive yield, i.e., E/Y, we present a series of plots (Figs. B1-B24) showing how E/Y changes as the medium's water content or saturation is varied while the total porosity or gas fill porosity is held fixed and vice versa. We assume in all instances that the medium properties are restricted to the ranges shown in Table B1.

In addition to the plots of E/Y (x,y) vs x at fixed y (where x and y are chosen from ϕ, ϕg, W, and K), we also present plots of

$$\frac{d}{dx}\frac{E}{Y}(x,y) \equiv \frac{\partial}{\partial\gamma}\frac{E}{Y}(\gamma)\,\frac{\partial\gamma}{\partial x}(x,y) = \frac{8}{(3\gamma-1)^2}\,\frac{\partial\gamma}{\partial x}(x,y) \ .$$

In particular, we plot $\frac{d}{dx}$ E/Y (x,y) vs x at fixed y and vs y at fixed x in order to more clearly show how E/Y is affected by variations in medium properties.

Inspection of the plots presented in this appendix shows some unexpected results. In particular, it is seen that the effect of increasing the water content or saturation while holding porosity fixed changes depending on the value of porosity being considered. For the silicate type rock being considered, increasing water content or saturation while porosity is held fixed at a value less than 0.325 (32.5%) actually results in a slight decrease in energy coupling. For porosities greater than 0.325, increasing water content or saturation results in increased coupling efficiency, and at porosity exactly equal to 0.325 it seems that water content and porosity have no effect on the energy coupled from the explosion to the shock wave.

This somewhat surprising dependence of the influence of water content and saturation on the value of porosity being considered follows from the use of Eq. (19) to define γ. This same effect was noted in a previous study of the Gruneisen coefficient for wet, porous materials.[11,12] The effect is evidence of a tradeoff between the lubricating effect of the water upon the grains of matrix material and the incompressibility of the water itself.

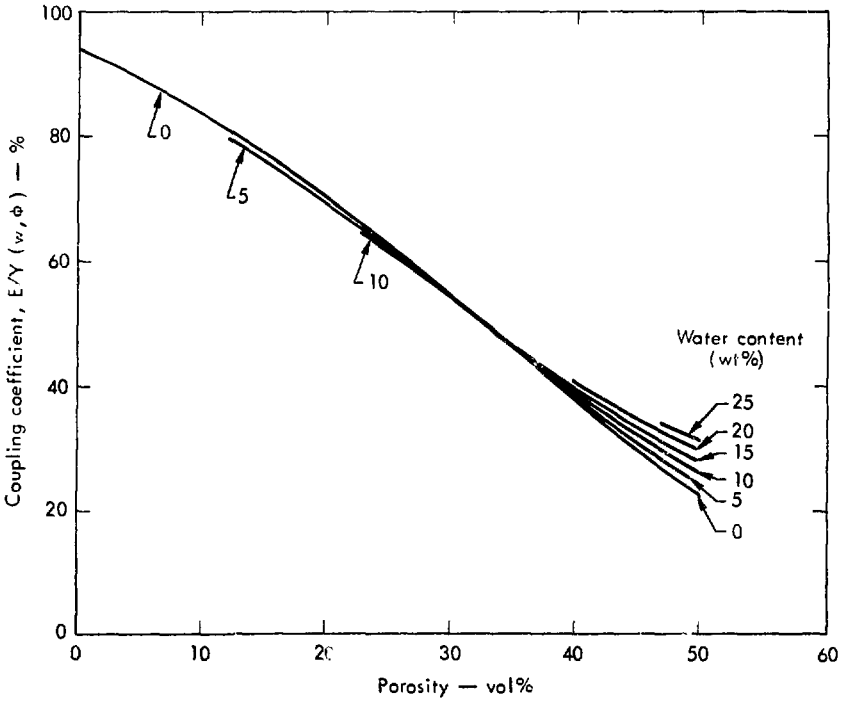

Fig. B1 $\frac{E}{Y}(W,\phi)$ is shown for fixed values of W and varying ϕ.

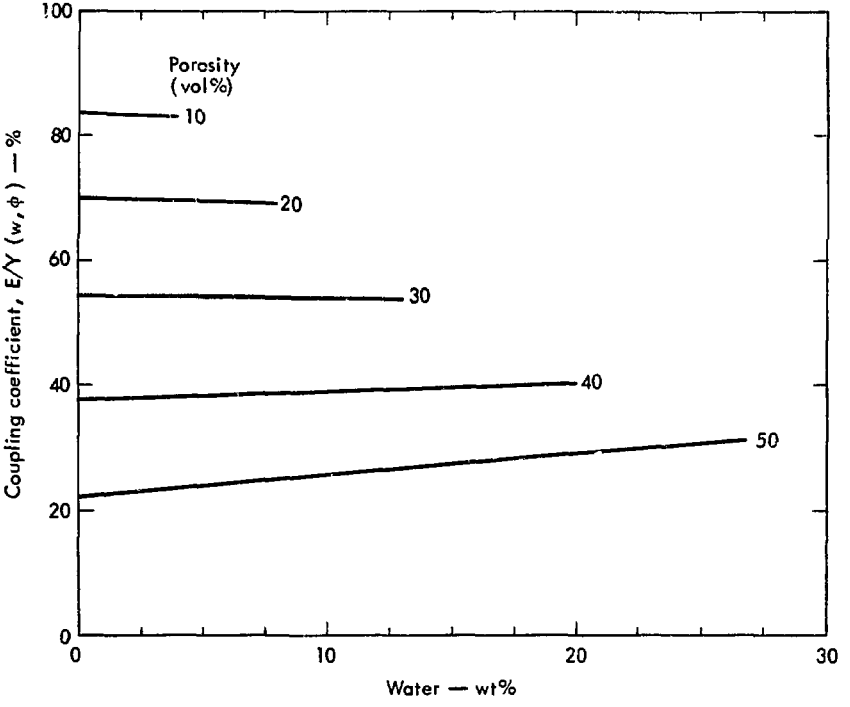

Fig. B2 $\frac{E}{Y}(W,\phi)$ is shown for fixed values of ϕ and varying W.

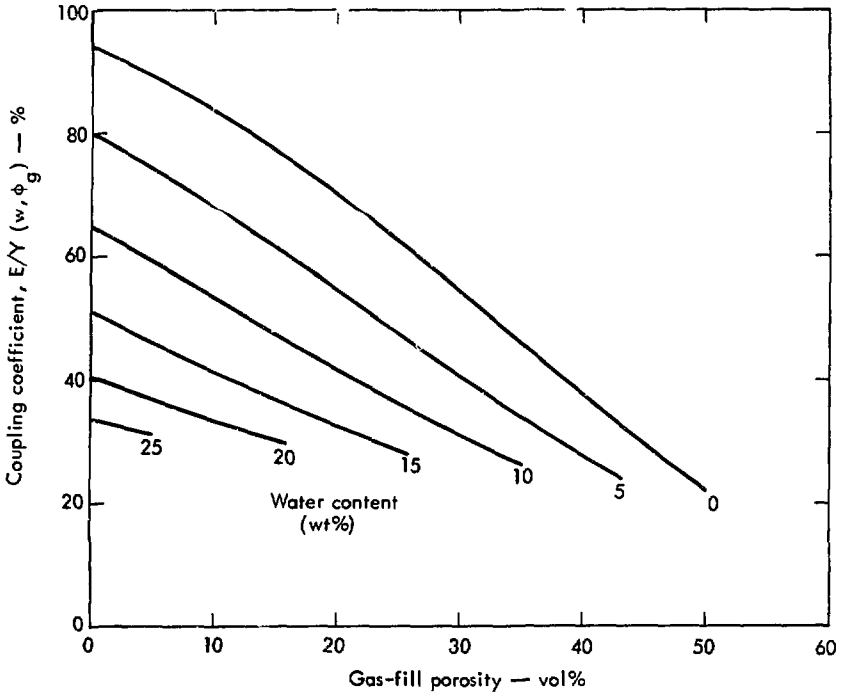

Fig. B3 $\frac{E}{Y}(W,\phi_g)$ is shown for fixed values of W and varying ϕ_g.

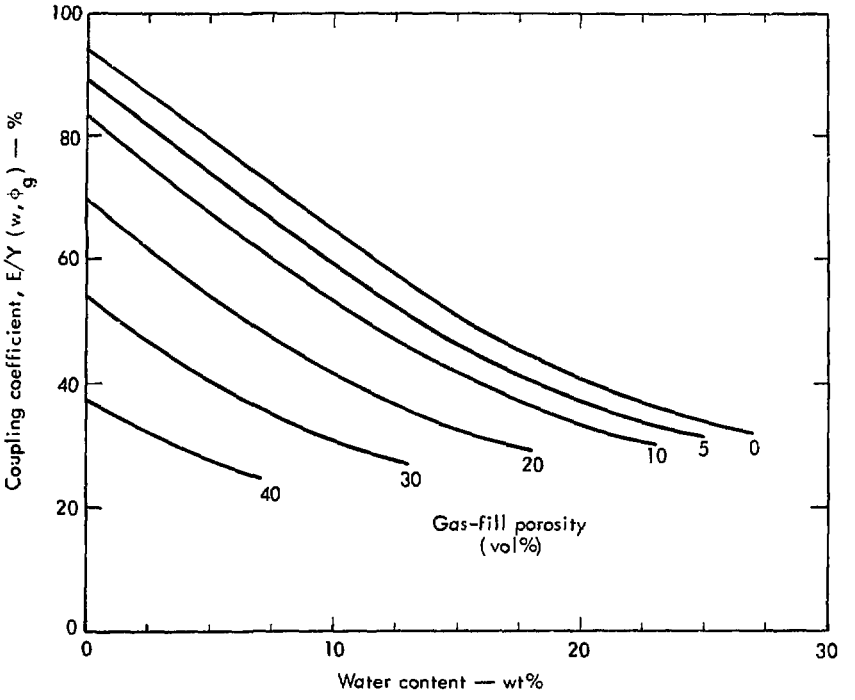

Fig. B4 $\frac{E}{Y}(W,\phi_g)$ is shown for fixed values of ϕ_g and varying W.

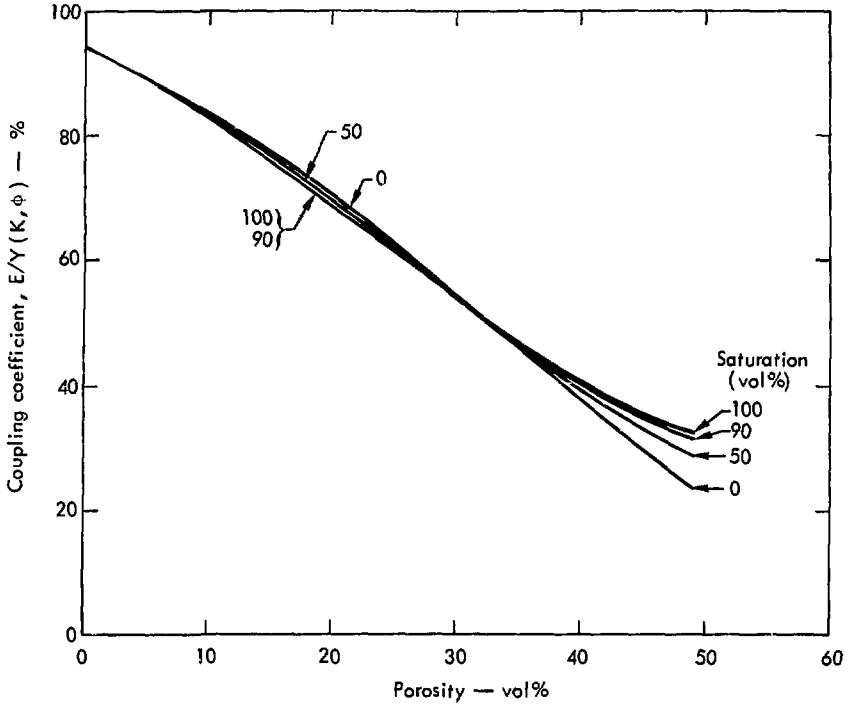

Fig. B5 $\frac{E}{Y}(K,\phi)$ is shown for fixed values of K and varying ϕ.

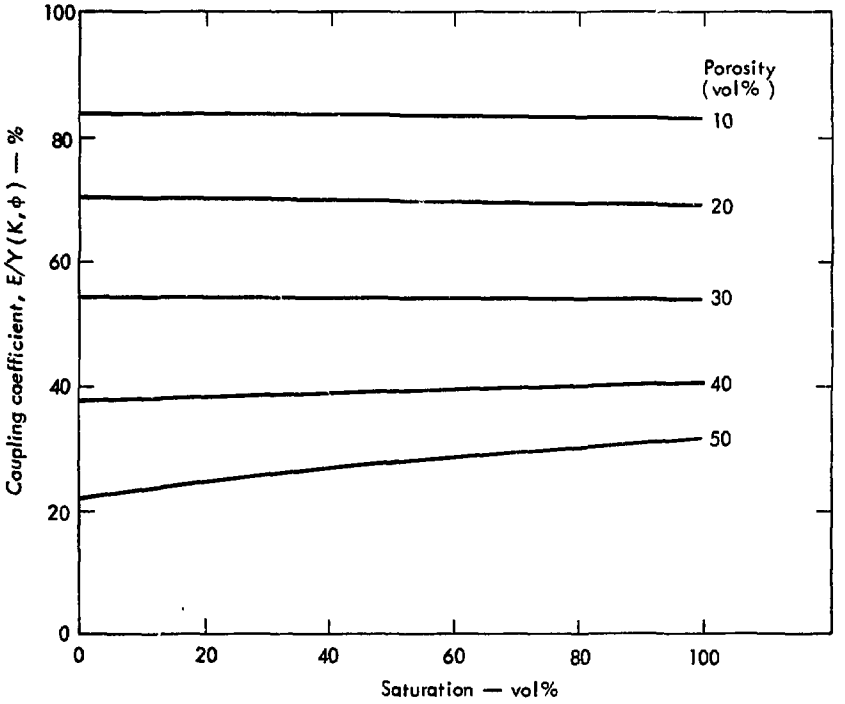

Fig. B6 $\frac{E}{Y}(K,\phi)$ is shown for fixed values of ϕ and varying K.

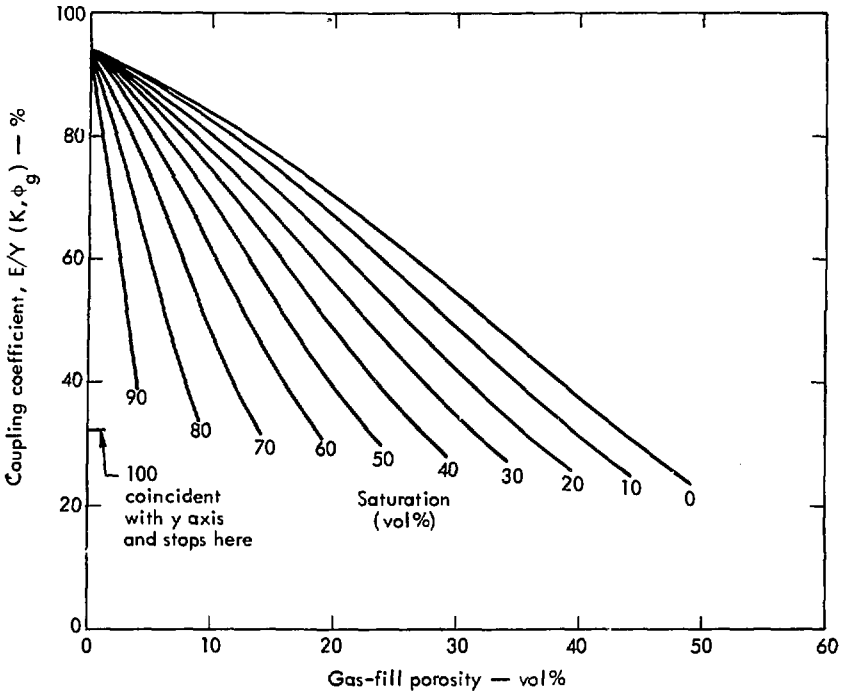

Fig. B7 $\frac{E}{Y}$ (K,ϕ_g) is shcwn for fixed values of K and varying ϕ_g.

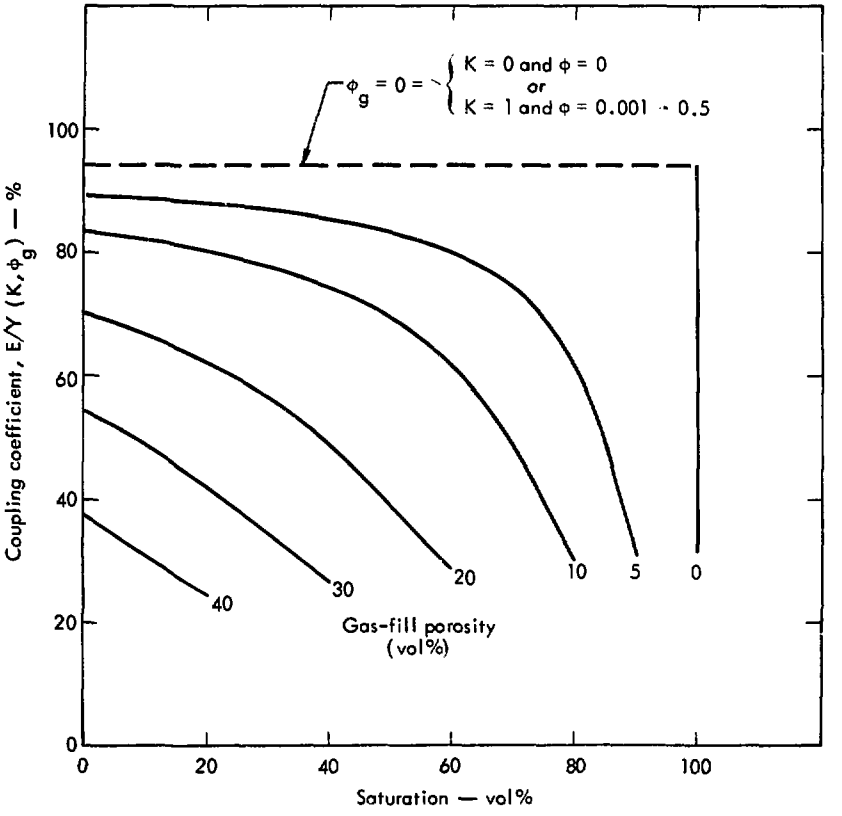

Fig. B8 $\frac{E}{Y}(K,\phi_g)$ is shown for fixed values of ϕ_g and varying K.

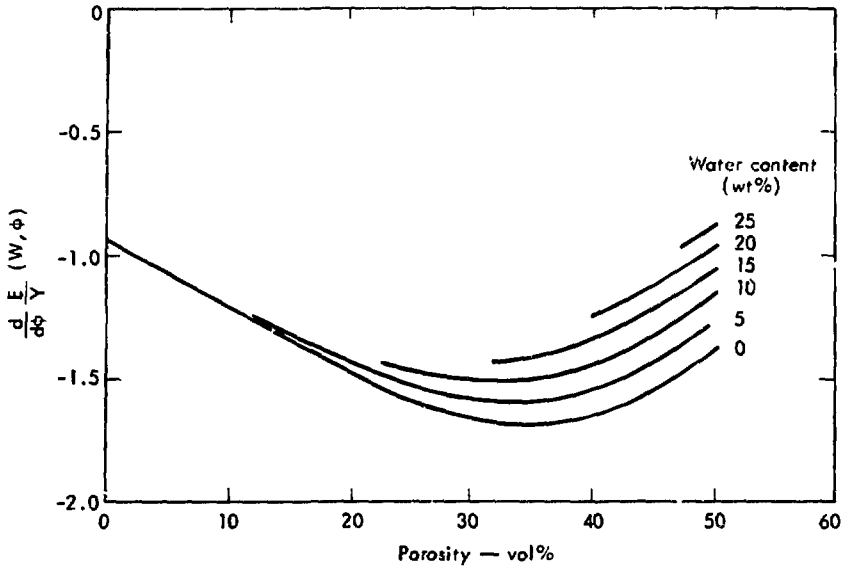

Fig. B9 $\frac{d}{d\phi}\frac{E}{Y}(W,\phi)$ is shown for fixed values of W and varying ϕ.

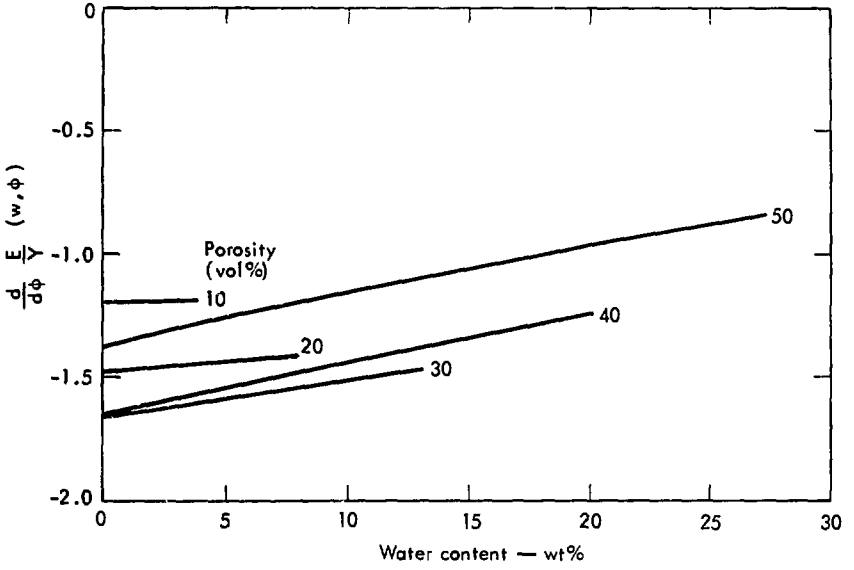

Fig. B10 $\frac{d}{d\phi}\frac{E}{Y}(W,\phi)$ is shown for fixed values of ϕ and varying W.

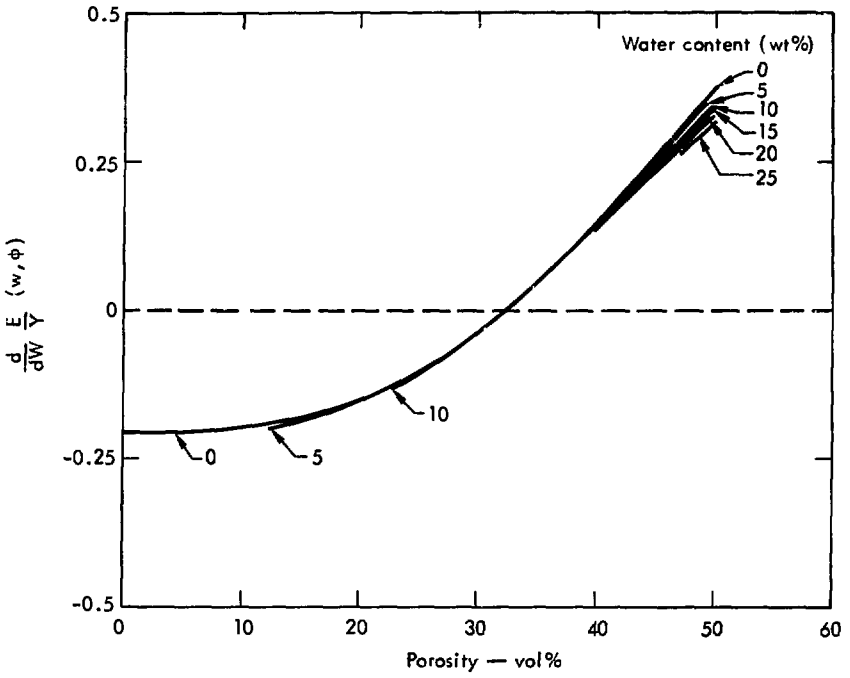

Fig. B11 $\frac{d}{dW}\frac{E}{Y}(W,\phi)$ is shown for fixed values of W and varying ϕ.

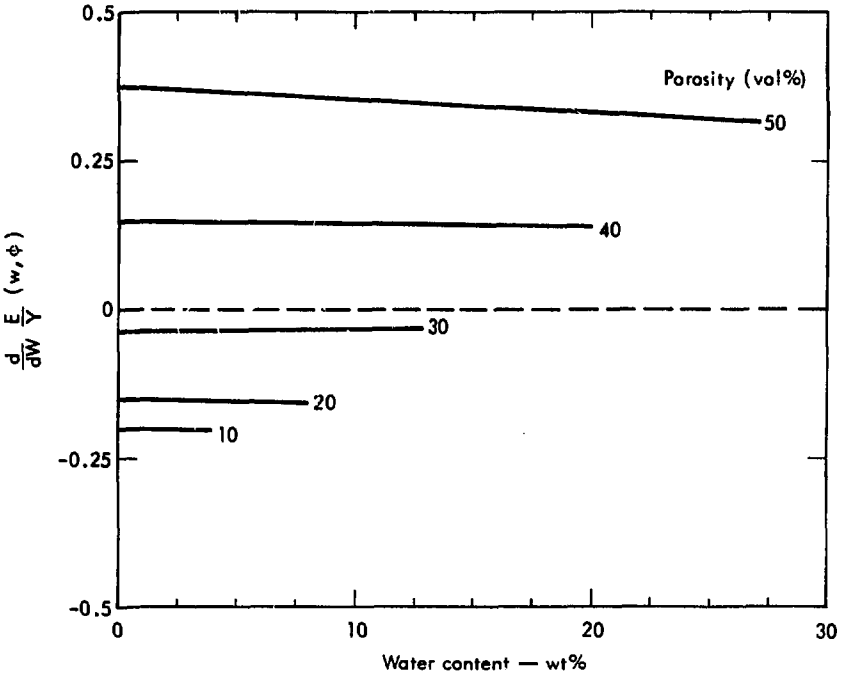

Fig. B12 $\frac{d}{dW}\frac{E}{Y}(W,\phi)$ is shown for fixed values of ϕ and varying W.

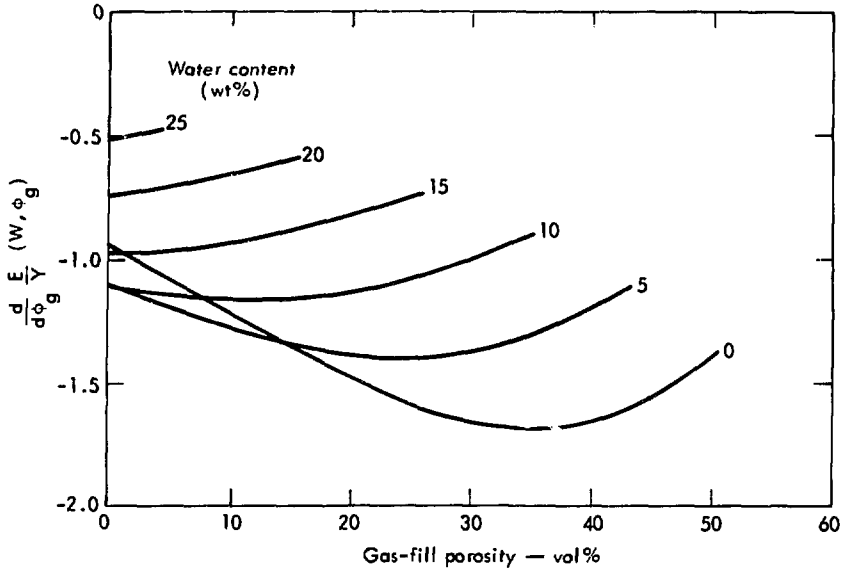

Fig. B13 $\frac{d}{d\phi_g}\frac{E}{Y}(W,\phi_g)$ is shown for fixed values of W and varying ϕ_g.

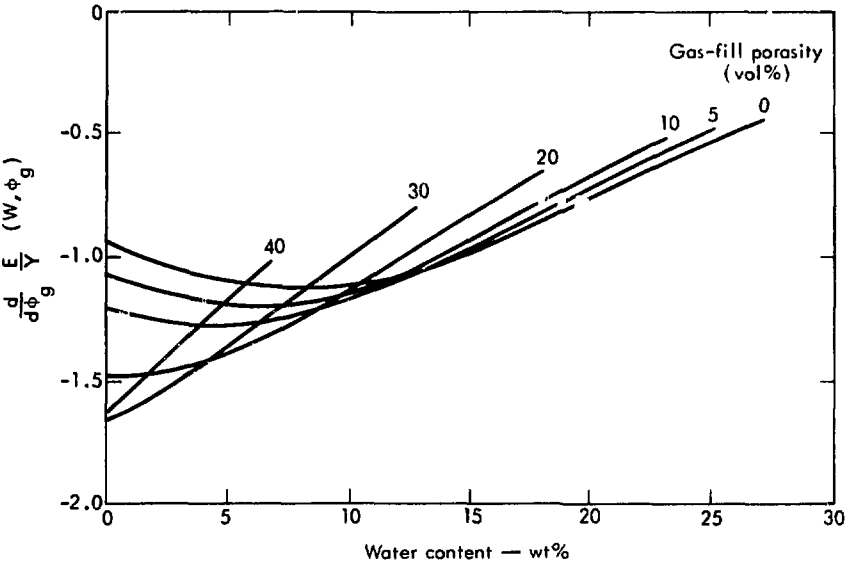

Fig. B14 $\frac{d}{d\phi_g}\frac{E}{Y}(W,\phi_g)$ is shown for fixed values of ϕ_g and varying W.

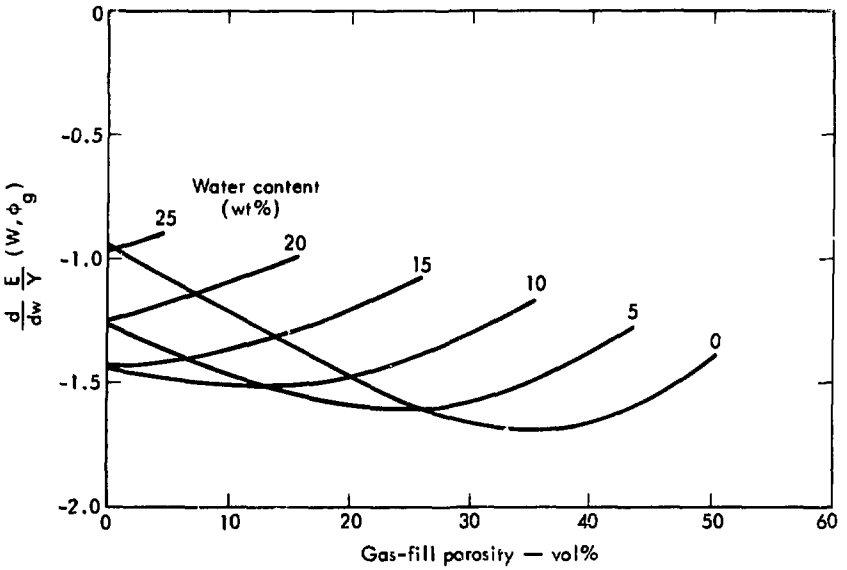

Fig. B15 $\frac{d}{dW}\frac{E}{Y}(W,\phi_g)$ is shown for fixed values of W and varying ϕ_g.

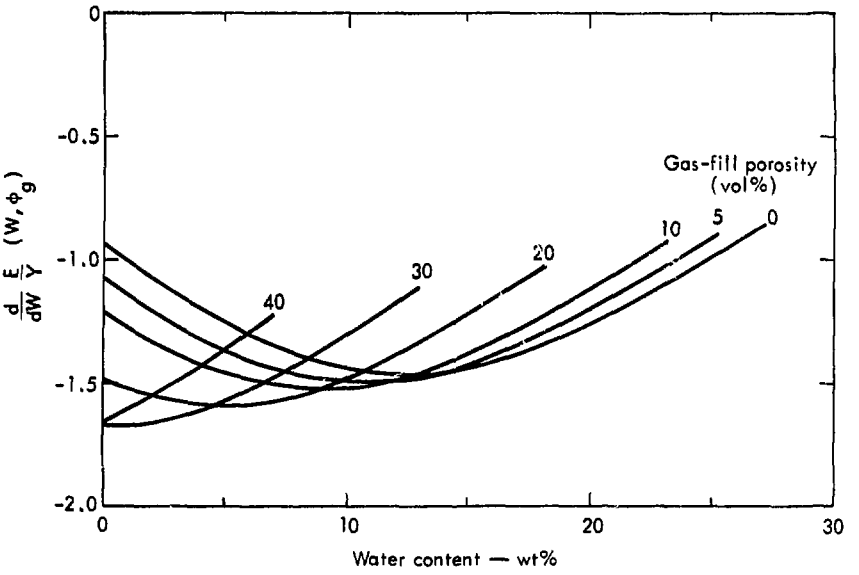

Fig. B16 $\frac{d}{dW}\frac{E}{Y}(W,\phi_g)$ is shown for fixed values of ϕ_g and varying W.

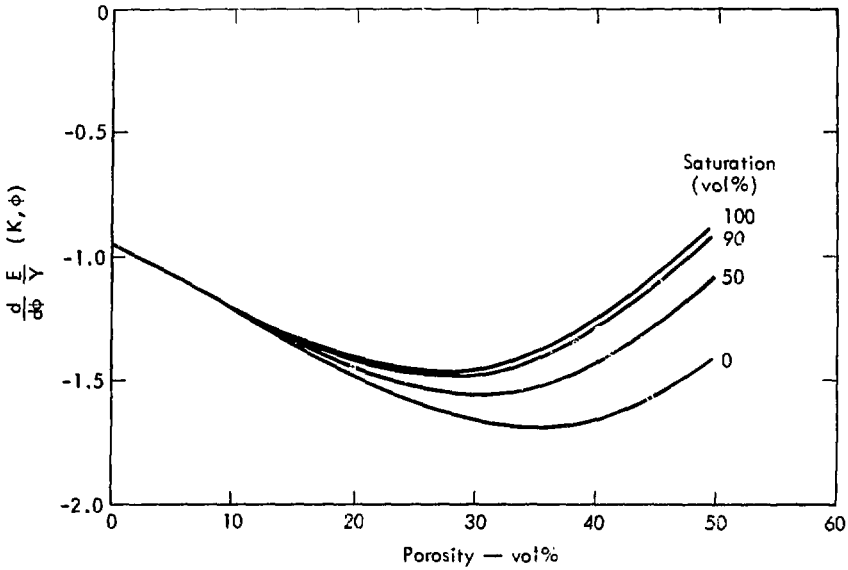

Fig. B17 $\frac{d}{d\phi}\frac{E}{Y}(K,\phi)$ is shown for fixed values of K and varying ϕ.

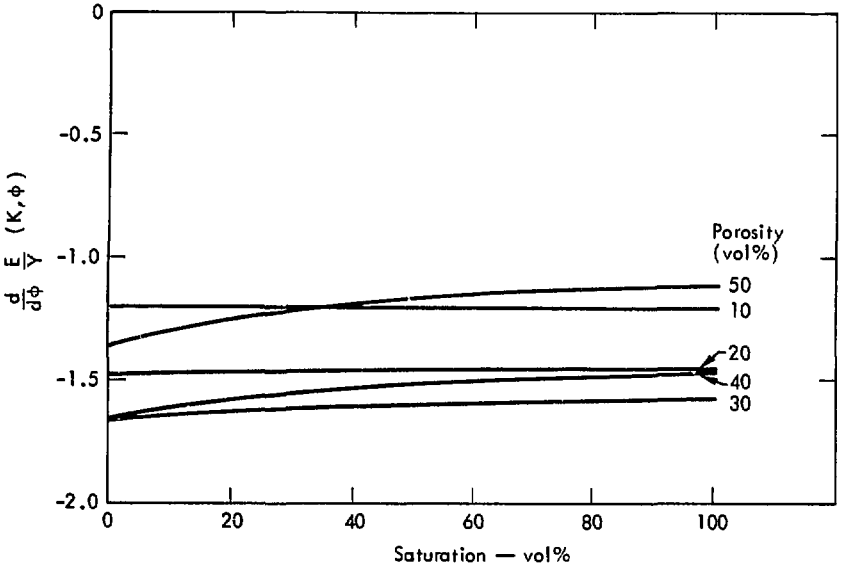

Fig. B18 $\frac{d}{d\phi}\frac{E}{Y}(K,\phi)$ is shown for fixed values of ϕ and varying K.

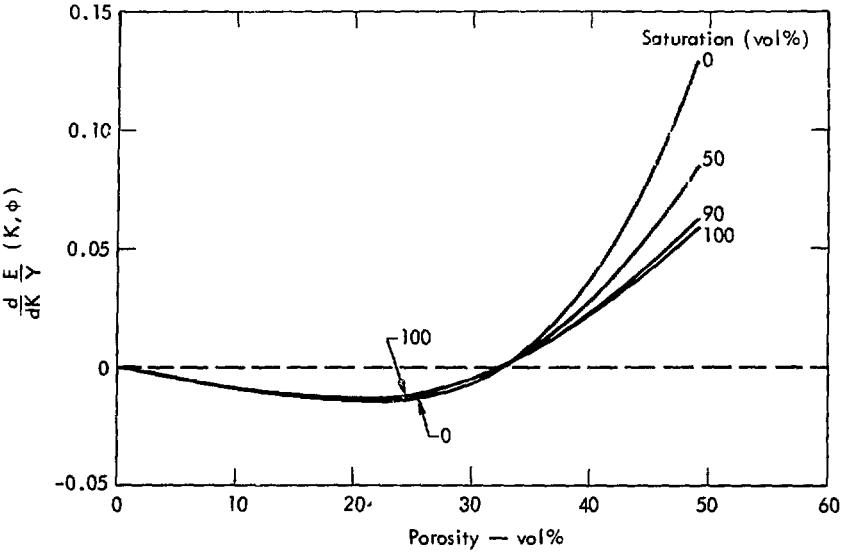

Fig. B19 $\frac{d}{dK}\frac{E}{Y}(K,\phi)$ is shown for fixed values of K and varying ϕ.

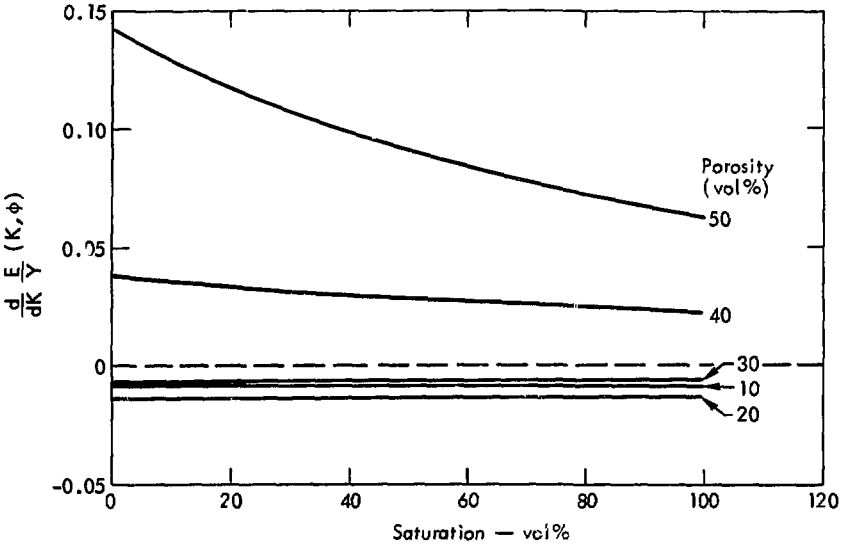

Fig. B20 $\frac{d}{dK}\frac{E}{Y}(K,\phi)$ is shown for fixed values of ϕ and varying K.

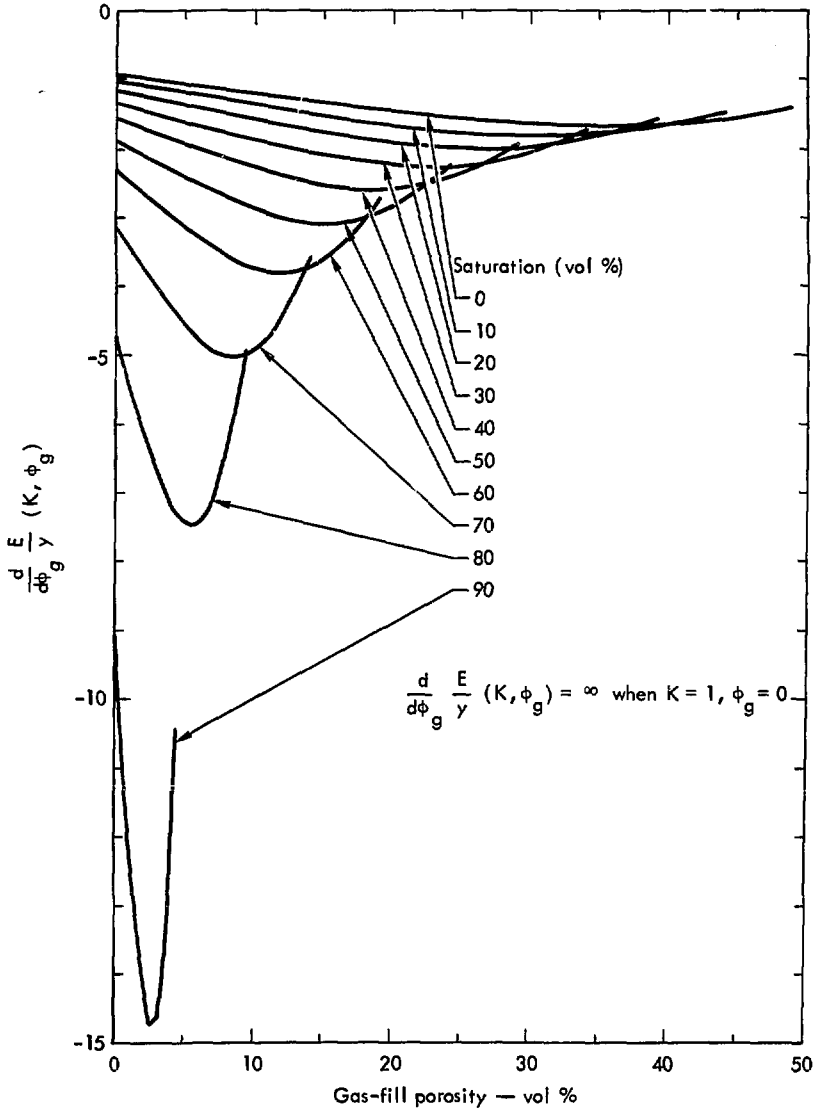

Fig. B21 $\frac{d}{d\phi_g}\frac{E}{Y}(K,\phi_g)$ is shown for fixed values of K and varying ϕ_g.

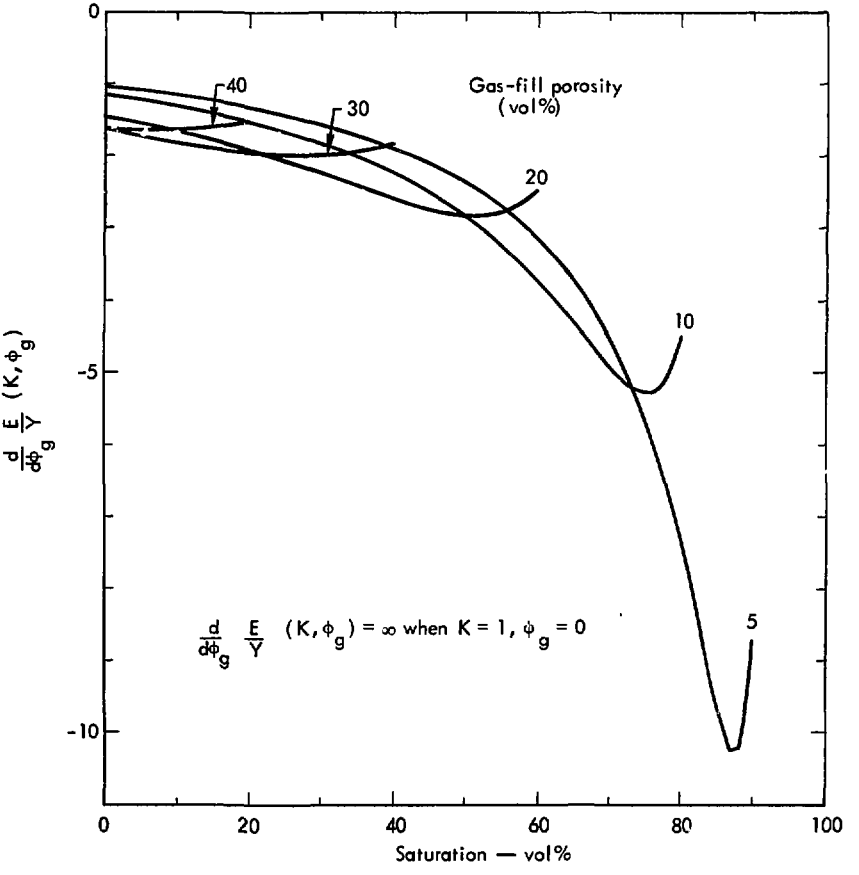

Fig. B22 $\frac{d}{d\phi_g}\frac{E}{Y}(K,\phi_g)$ is shown for fixed values of ϕ_g and varying K.

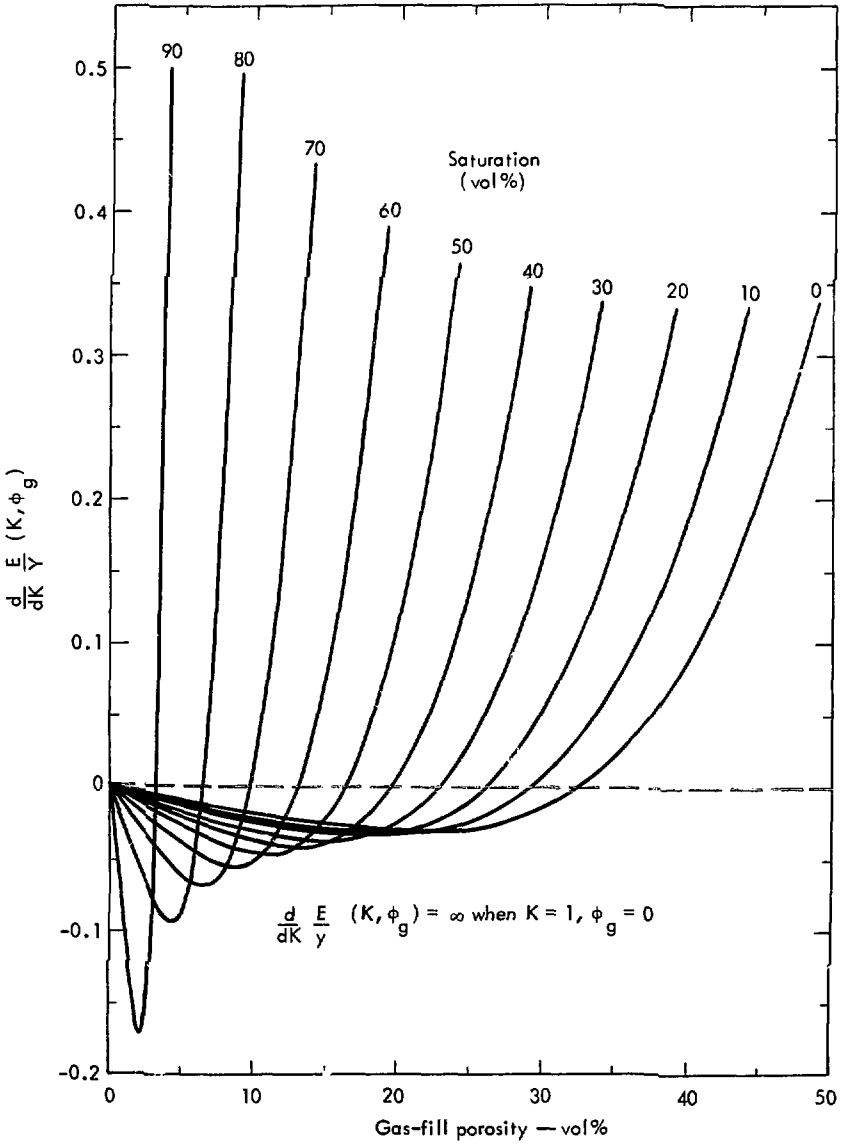

Fig. B23 $\frac{d}{dK}\frac{E}{Y}(K,\phi_g)$ is shown for fixed values of K and varying ϕ_g.

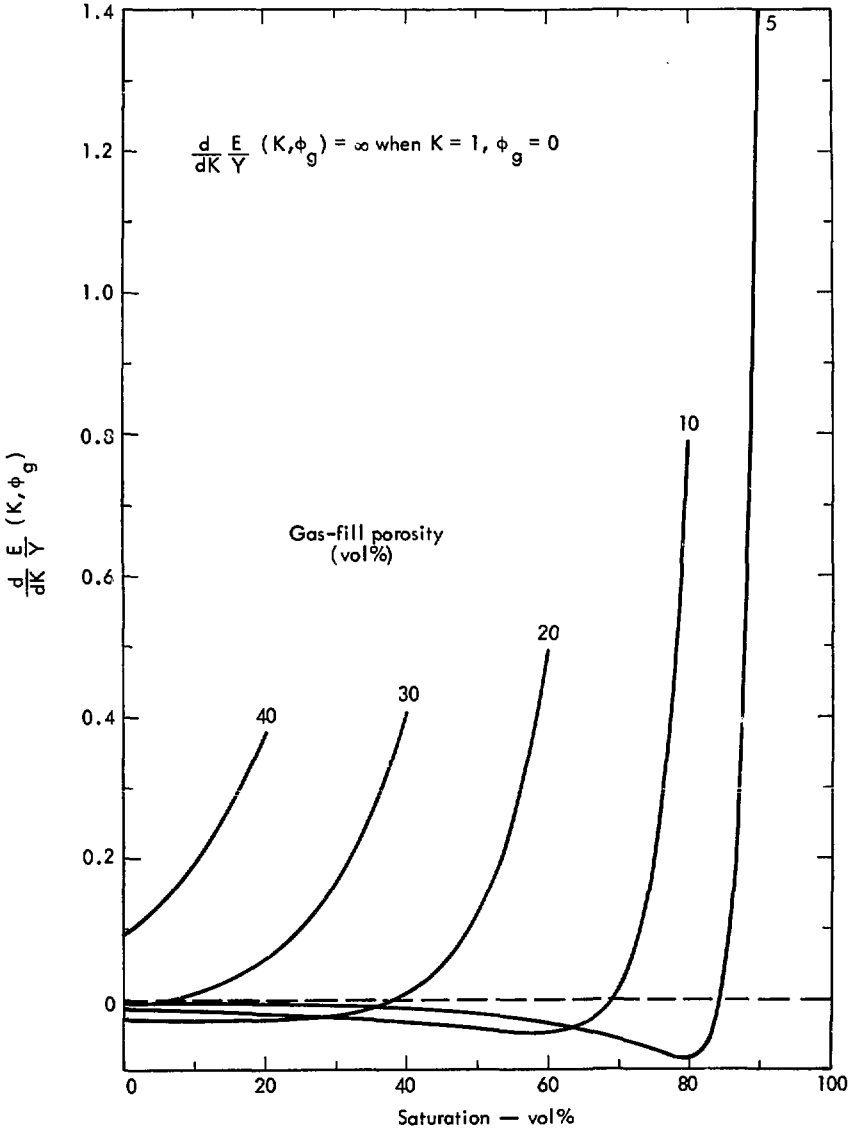

Fig. B24 $\frac{d}{dK}\frac{E}{Y}(K,\phi_g)$ is shown for fixed values of ϕ_g and varying K.

Table B1 Range of medium properties assumed.

Property	Range of values	Units
S	1.3	–
Grain density (ρ_g)	2.65	Mg/m^3
Total porosity (ϕ)	0 – 50	vol %
Gas-fill porosity (ϕ_g)	0 – 50	vol %
Water content (W)	0 – 27	wt %
Saturation (K)	0 – 100	vol %

RBC/jb/lmc